Force-gradient sensitive Kelvin probe force microscopy by dissipative electrostatic force modulation

Yoichi Miyahara[a] and Peter Grutter
Department of Physics, McGill University, 3600 rue University, Montreal, Quebec H3A 2T8, Canada

(Received 28 February 2017; accepted 10 April 2017; published online 20 April 2017)

We report a Kelvin probe force microscopy (KPFM) implementation using the dissipation signal of a frequency modulation atomic force microscopy that is capable of detecting the gradient of electrostatic force rather than electrostatic force. It features a simple implementation and faster scanning as it requires no low frequency modulation. We show that applying a coherent ac voltage with two times the cantilever oscillation frequency induces the dissipation signal proportional to the electrostatic force gradient which depends on the effective dc bias voltage including the contact potential difference. We demonstrate the KPFM images of a MoS_2 flake taken with the present method are in quantitative agreement with those taken with the frequency modulated Kelvin probe force microscopy technique. *Published by AIP Publishing.* [http://dx.doi.org/10.1063/1.4981937]

We recently reported a Kelvin probe force microscopy (KPFM) implementation (D-KPFM) in which the dissipation signal of a frequency modulation atomic force microscopy (FM-AFM) is used for dc-bias voltage feedback.[1] In KPFM, a contact potential difference (CPD) between the tip and sample, V_{cpd}, is measured by finding a dc bias voltage, V_{bias}, nullifying a capacitive electrostatic force, F_{elec}, which is proportional to the effective dc potential difference $V_{dc} \equiv (V_{bias} - V_{cpd})$. In order to detect F_{elec} in the presence of other force components such as van der Waals force and chemical bonding force, F_{elec} is usually modulated by superposing an ac bias voltage to V_{bias}, and the resulting modulated component of the measured force (or force gradient) is detected by lock-in detection.[2] While the modulated frequency shift signal is used in the case of the conventional KPFM with FM-AFM (FM-KPFM),[3] in D-KPFM, F_{elec} is detected through the dissipation signal of FM-AFM, which is the amplitude of cantilever excitation signal. The dissipation is induced by applying a coherent sinusoidal ac voltage with the frequency of the tip oscillation, which is 90° out of phase with respect to the tip oscillation. The induced dissipation signal can be used for KPFM voltage feedback loop as it is proportional to the effective dc potential difference, V_{dc}.

Here, we report another D-KPFM implementation (2ω D-KPFM) where the induced dissipation is proportional to the electrostatic force gradient, resulting in the identical potential image contrast as is obtained by FM-KPFM. In 2ω D-KPFM, the frequency of the applied ac voltage is two times that of tip oscillation.

The electrostatic force between two conductors connected to an ac and dc voltage source, F_{elec}, is described as follows:[4]

$$\begin{aligned} F_{elec} &= \frac{1}{2}\frac{\partial C}{\partial z}\{V_{bias} - V_{cpd} + V_{ac}\cos(\omega_{el}t + \phi)\}^2 \\ &= \alpha\{V_{dc} + V_{ac}\cos(\omega_{el}t + \phi)\}^2, \end{aligned} \tag{1}$$

where C is the tip-sample capacitance and $\alpha \equiv \frac{1}{2}\frac{\partial C}{\partial z}$. V_{ac} and ω_{el} are the amplitude, angular frequency of the ac bias voltage and ϕ is the phase of the ac bias voltage with respect to the tip oscillation. z is the position of the tip and is oscillating around its mean position from the sample, z_0, expressed as $z(t) = z_0 + A\cos(\omega_m t)$ with ω_m and A being its oscillation angular frequency and amplitude, respectively. In FM-AFM, the AFM cantilever is self-oscillated by a driving force such as piezoacoustic or photothermal excitation[5] such that the oscillation frequency, $f_m = \omega_m/2\pi$, tracks its resonance frequency with $f_m = f_0$, using a positive feedback circuit equipped with an amplitude controller.[6] The frequency shift, Δf, and dissipation signal, g, are expressed as follows:[7–9]

$$\Delta f \approx -\frac{f_0^2}{kA}\int_0^{2\pi/\omega_m} F_{ts}(t)\cos(\omega_m t)dt, \tag{2}$$

$$g \approx \frac{1}{Q} + \frac{2f_0^2}{kA}\int_0^{2\pi/\omega_m} F_{ts}(t)\sin(\omega_m t)dt, \tag{3}$$

where k and Q are the spring constant and quality factor of the cantilever. This indicates that Δf and g are proportional to the Fourier in-phase (even), F_{in}, and quadrature (odd), F_{quad}, coefficients of the fundamental harmonic component (in this case ω_m) of the oscillating tip-sample interaction force, $F_{ts}(t)$, respectively. This yields $\Delta f = -\frac{1}{2}\frac{f_0}{kA}F_{in}$ and $g = g_0(1 + \frac{Q}{kA}F_{quad})$, where g_0 is the dissipation signal determined by the intrinsic dissipation of the cantilever. As we have already pointed out,[1] the distance dependence of $\alpha(z) \equiv \frac{1}{2}\frac{\partial C}{\partial z}(z)$ has to be taken into account in order to obtain the correct forms of F_{in} and F_{quad} acting on the oscillating tip that is subject to the coherent oscillating electrostatic force. It is the interaction between the mechanical oscillation of the tip and the coherent oscillating electrostatic force that leads to the following results.[10] Here, we consider the case of $\omega_{el} = 2\omega_m$ which has previously been suggested by Nomura *et al.*[11] for a similar but different KPFM implementation with dissipative electrostatic force modulation.[12] By expanding $\alpha(z)$ around the mean tip position, z_0, and taking the first

[a]Author to whom correspondence should be addressed. Electronic mail: yoichi.miyahara@mcgill.ca

order term, α is expressed as $\alpha(z) \approx \alpha(z_0) + \alpha' \times (z - z_0) = \alpha_0 + \alpha' A \cos(\omega_m t)$. Substituting this into Eq. (1) with setting $\omega_{el} = 2\omega_m$ and gathering all the terms with ω_m components yields the following result (detailed derivation available in supplementary material):

$$\begin{aligned} F_{\omega_m}(t) &= \alpha' A \left\{ \left(V_{dc}^2 + \frac{V_{ac}^2}{2} \right) \cos(\omega_m t) + V_{dc} V_{ac} \cos(\omega_m t + \phi) \right\} \\ &= \alpha' A \left\{ V_{dc}^2 + \cos(\phi) V_{dc} V_{ac} + \frac{V_{ac}^2}{2} \right\} \cos(\omega_m t) \\ &\quad - \alpha' A V_{dc} V_{ac} \sin(\phi) \sin(\omega_m t) \\ &= F_{in} \cos(\omega_m t) + F_{quad} \sin(\omega_m t), \end{aligned}$$

where

$$F_{in} = \alpha' A \left(V_{dc} + \frac{V_{ac}}{2} \cos\phi \right)^2 + \frac{\alpha' A}{2} \left(1 - \frac{\cos^2\phi}{2} \right) V_{ac}^2, \quad (4)$$

$$F_{quad} = -\alpha' A V_{dc} V_{ac} \sin\phi. \quad (5)$$

We notice that F_{quad} is proportional to α' rather than α, indicating F_{quad} is now sensitive to the electrostatic force gradient. It is interesting to notice that the apparent shift of V_{cpd} is just determined by ϕ and V_{ac} and does not depend on α in contrast to the previously reported D-KPFM (1ωD-KPFM) (see Eqs. (11)–(13) in Ref. 1). A key aspect of this technique is the absence of such a shift in F_{quad} for any ϕ, which is advantageous as the accurate setting of ϕ is not required for accurate CPD measurements. ϕ just affects the magnitude of F_{quad}, which determines the signal-to-noise ratio of the CPD measurements. When $\phi = 90°$, we obtain

$$F_{in} = \alpha' A \left(V_{dc}^2 + \frac{V_{ac}^2}{2} \right) = \alpha' A (V_{bias} - V_{cpd})^2 + \frac{\alpha' A}{2} V_{ac}^2$$

$$F_{quad} = -\alpha' A V_{dc} V_{ac} = -\alpha' A (V_{bias} - V_{cpd}) V_{ac}.$$

In this case, the apparent shift of CPD in F_{in} vanishes, and the slope of F_{quad}–V_{bias} curve takes its maximum value. Notice that F_{quad} behaves exactly in the same way as the lock-in demodulated frequency shift signal used in FM-KPFM. F_{quad} is, however, available directly in the dissipation signal without the lock-in demodulation, enabling the faster KPFM feedback. When $V_{bias} = V_{cpd}$, the dissipation signal turns back to its original value, g_0. It is therefore possible to use the dissipation signal, g, for the KPFM bias voltage feedback by choosing g_0 as its control setpoint value.

Figure 1 depicts the block diagram of the experimental setup used for both 1ω and 2ωD-KPFM measurements. The setup is based on the self-oscillation mode FM-AFM system,[6] and three additional components, a frequency doubler, a phase shifter, a proportional-integrator (PI) controller, are required for 2ωD-KPFM operation. The amplitude controller composed of a root-mean-square (RMS) amplitude detector, and a PI controller is used to keep an oscillation amplitude constant. The output of the amplitude controller is the dissipation signal which is used for controlling V_{bias}. The detection bandwidth of the RMS amplitude detector is extended to about 3 kHz. In order to produce a sinusoidal ac voltage with two times the tip oscillation frequency, the sinusoidal deflection signal from the cantilever deflection sensor is first fed into a frequency doubler. Then, the output of the frequency doubler passes through the additional phase shifter (Phase Shifter 2), which serves to adjust the phase of the ac voltage, ϕ. The dissipation signal acts as the input signal to the PI controller, which adjusts V_{bias} to maintain a constant dissipation equal to the value without V_{ac} applied, g_0.[13]

We used a JEOL JSPM-5200 atomic force microscope for the experiments with the modifications described in Ref. 1. An open source scanning probe microscopy control software GXSM was used for the control and data acquisition.[14] A commercial silicon AFM cantilever (NSC15, MikroMasch) with a typical spring constant of about 28 N/m and resonance frequency of ~300 kHz was used in high-vacuum environment with the pressure of 1×10^{-7} mbar.

In order to validate Eqs. (4) and (5), Δf–V_{bias} and g–V_{bias} curves were measured while a coherent sinusoidally oscillating voltage with $\omega_{el} = 2\omega_m$, $V_{ac} = 1$ V (2 $V_{p\text{-}p}$) and various phases, ϕ, is superposed with V_{bias}. Figures 2(a) and 2(b) show simultaneously measured Δf and g versus V_{bias} curves, respectively. The curves are taken on a template stripped gold surface. A fitted curve with a parabola for each of the Δf–V_{bias} curves (Eq. (4)) or with a linear line for each of the g–V_{bias} curves (Eq. (5)) is overlaid on each experimental curve, indicating a very good agreement between the theory and experiments. As can be seen in Figs. 2(a) and 2(b), the position of the parabola vertex shifts both in V_{bias} and Δf axes and the slope of g–V_{bias} curve changes systematically

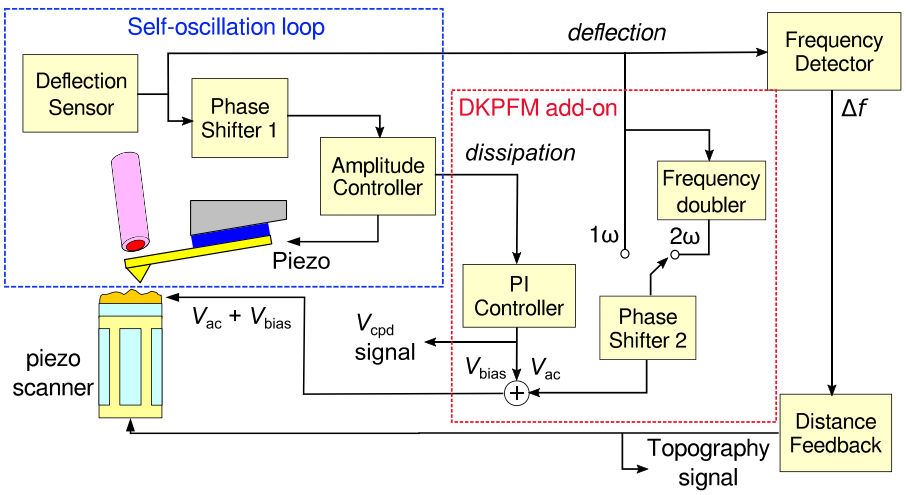

FIG. 1. Block diagram of the experimental setup for force-gradient sensitive D-KPFM measurements.

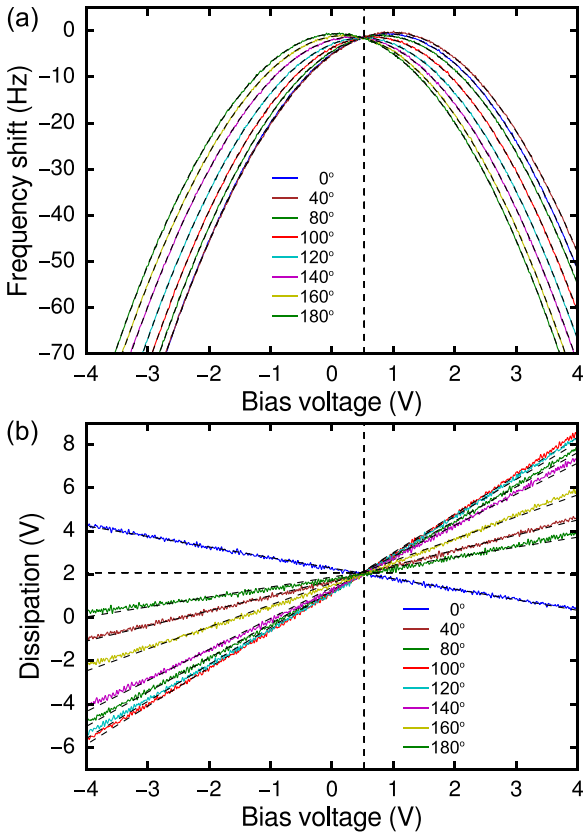

FIG. 2. (a) Frequency shift, Δf, and (b) dissipation signal, g, versus dc bias voltage, V_{bias}, curves taken with a coherent sinusoidally oscillating voltage with $\omega_{\text{el}} = 2\omega_{\text{m}}$, $V_{\text{ac}} = 1$ V and various ϕ, applied to a template stripped gold substrate. The vertical dashed line in (a) and (b) indicates V_{cpd}, which is measured as the voltage coordinate of the parabola vertex without V_{ac}. The horizontal dashed line in (b) indicates the dissipation without V_{ac}. In both figures, each of dashed lines represents fitted curves assuming a parabola for Δf and a linear line for g as indicated in Eqs. (4) and (5), respectively. The oscillation amplitude of the tip was 10 $\text{nm}_{\text{p-p}}$, and the quality factor of the cantilever was 25 000.

with the varied phase, ϕ. For further validating the theory, the voltage coordinate of the parabola vertex (parabola minimum voltage) of each Δf–V_{bias} curve and the slope of each g–V_{bias} curve are plotted against ϕ in Fig. 3. Each plot is overlaid with a fitted curve (solid curve) with the cosine function (see Eq. (4)) for the parabola minimum voltage and with the sine function (Eq. (5)) for the dissipation slope, demonstrating an excellent agreement between the experiment and theory. The V_{bias} dependence of the frequency shift coordinate of the parabola vertices (frequency shift offset) also shows a very good agreement with the theory (second term of Eq. (4)). (The fitting result is available in supplementary material.) The parabola minimum voltage versus phase curve intersects that of Δf–V_{bias} without ac bias voltage at $\phi = 121°$. The deviation from the theoretically predicted value of 90° is due to the phase delay in the detection electronics. We also notice that the amplitude of parabola minimum versus phase curve is 0.472 V, which is in good agreement with 0.5 V predicted by the theory ($V_{\text{ac}}/2$ in Eq. (4)).

Figure 4 shows topography and CPD images of a patterned MoS_2 flake exfoliated on SiO_2/Si substrate taken by (a) and (d) 1ωD-KPFM, (b) and (e) 2ω D-KPFM, and (c) and (f) FM-KPFM techniques taken with the same tip, respectively. In 1ω (2ω) D-KPFM imaging, a sinusoidally

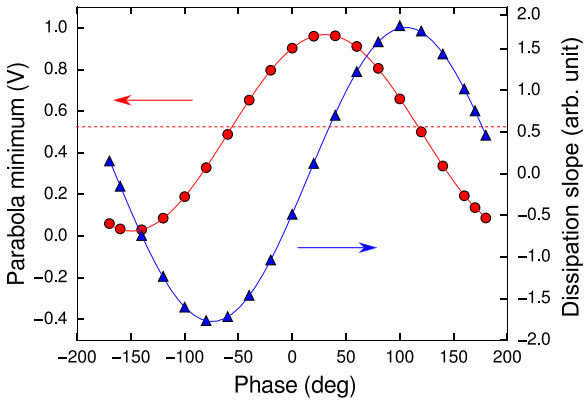

FIG. 3. Voltage coordinate of the vertices of the measured Δf-V_{bias} curves (parabola minimum) (red circles) extracted from the results in Fig. 2(a), and the slope of dissipation-V_{bias} curves (blue triangles) extracted from Fig. 2(a). Each solid line represents the fitted curve with the cosine function (Eq. (4)) for the parabola minimum and with the sine function (Eq. (5)) for the dissipation slope. The horizontal dashed line indicates the voltage coordinate of the parabola measured without the ac bias voltage.

oscillating voltage with $\omega_{\text{el}} = \omega_{\text{m}}$ ($\omega_{\text{el}} = 2\omega_{\text{m}}$), $V_{\text{ac}} = 50$ mV ($V_{\text{ac}} = 1$ V), and $\phi = 22°$ ($\phi = 18°$) coherent with the tip oscillation was applied to the sample. In FM-KPFM imaging, a sinusoidally oscillating voltage with $\omega_{\text{el}} = 300$ Hz and $V_{\text{ac}} = 1$ V was applied to the sample. The detection bandwidth of the lock-in was 100 Hz, which is chosen below the bandwidth of the frequency detector (400 Hz). The scanning time for all the images was 1 s/line. A stripe pattern with 2 μm pitch was created by reactive ion etching on the MoS_2 flake. The topography images show an unetched terrace located between the etched regions. The height of the unetched terrace is approximately 20 nm with respect to the etched regions. The bands shown in the middle of the CPD images corresponds to the unetched terrace and show a clear fractal-like pattern, which can be ascribed to the residue of the etch resist (PMMA). All three CPD images show apparently a very similar pattern on the terrace. However, a close inspection of the line profile of each image shows that 2ωD-KPFM and FM-KPFM provide a very similar potential profile with almost the same contrast while 1ωD-KPFM shows a potential contrast about two times smaller than that of 2ωD-KPFM and FM-KPFM. The close similarity between 2ωD-KPFM and FM-KPFM originates from the fact that F_{quad} (Eq. (5)) is proportional to the force gradient as we have discussed earlier. Slightly larger potential contrast in 2ωD-KPFM compared with FM-KPFM is due to the faster feedback response of 2ωD-KPFM (the closed loop feedback bandwidth is measured to be around 1 kHz) by virtue of the absence of low frequency modulation,[1] which is a clear advantage of both D-KPFM techniques over FM-KPFM. The bandwidth of FM-KPFM is limited by the detection bandwidth of the lock-in amplifier which is used to detect the modulated frequency shift in the output of the frequency detector. The detection bandwidth of the frequency detector (typically <1 kHz) limits the frequency of the ac bias voltage which in turn limits the lock-in bandwidth to a few hundred Hz. The lower contrast of 1ωD-KPFM is ascribed to its sensitivity to electrostatic force rather than electrostatic force gradient, which results in a larger spatial average due to the stray capacitance, including the body of the tip and the cantilever.[11,15–18]

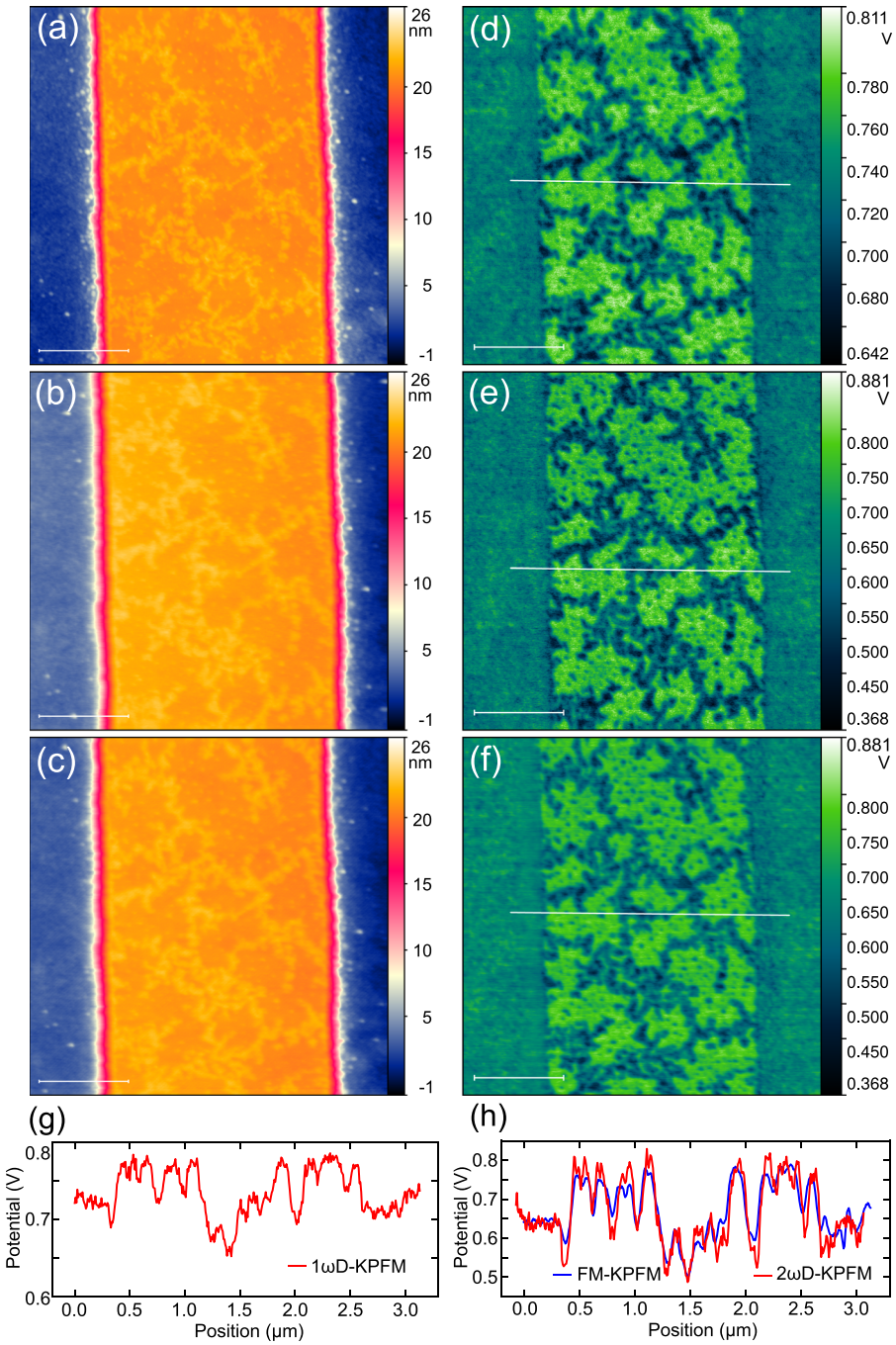

FIG. 4. Simultaneously taken topography (left raw) and CPD images (right raw) of patterned MoS_2 on SiO_2/Si substrate by (a) and (d) 1ωD-KPFM ($\Delta f = -10.3$ Hz, $A = 5\,\mathrm{nm_{p\text{-}p}}$, and $V_{ac} = 50$ mV), (b) and (e) 2ω D-KPFM ($\Delta f = -8.3$ Hz, $A = 5\,\mathrm{nm_{p\text{-}p}}$, and $V_{ac} = 1$ V), and (c) and (f) FM-KPFM ($\Delta f = -7.0$ Hz, $A = 5\,\mathrm{nm_{p\text{-}p}}$, $V_{ac} = 1$ V, and $f_{ac} = 300$ Hz). Scale bar is 1 μm. (g) Line profile of the 1ωD-KPFM potential image (d). (h) Line profile of the 2ωD-KPFM (e) (red) and FM-KPFM potential images (f) (blue).

In spite of a lower potential contrast, 1ωD-KPFM has an advantage that it requires much smaller $V_{ac} = 50$ mV compared with 1 V required in 2ωD-KPFM and FM-KPFM. This advantage is important for samples such as semiconductor where the influence of the large V_{ac} can be very important due to the band-bending effects. As it is easy to switch between 1ω and 2ωD-KPFM modes, 1ωD-KPFM can be used for qualitative measurement with less electrical disturbance while 2ωD-KPFM can be used to obtain more accurate CPD contrast on the same sample location. Another advantage of 2ωD-KPFM is that it is free from the capacitive crosstalk to the piezoelectric element and photodiode signal line[19] as the frequency of the ac voltage itself does not match any resonance of the cantilever.

In conclusion, we report a technique that enables force-gradient sensitive Kelvin probe force microscopy using the dissipation signal of FM-AFM for dc voltage feedback. It features the simpler implementation and faster scanning as it requires no low frequency modulation (no lock-in demodulation). The dissipation is caused by the oscillating electrostatic force that is coherent with the tip oscillation, which is induced by applying a sinusoidally oscillating ac voltage with the frequency two times that of the tip oscillation frequency. We theoretically analyzed the effect of the applied ac voltage and show that the induced dissipation is sensitive to electrostatic force gradient rather than electrostatic force. The experiments confirmed the theoretical analysis and demonstrated that 2ωD-KPFM provides essentially the same result obtained by FM-KPFM. The combination of 1ω and 2ωD-KPFM techniques will be a versatile tool to study the samples whose electrical properties are sensitive to the external electric field.

See supplementary material for the derivation of Eqs. (4) and (5), the experimental data of ϕ dependence of the frequency shift offset, and the optical micrograph of the MoS_2 sample.

The authors would like to thank Dr. Omid Salehzadeh Einabad and Professor Zetian Mi at McGill University for providing the MoS_2 sample. This work was partly supported by the Natural Science and Engineering Research Council (NSERC), le Fonds Québécois de Recherche sur la Nature et les Technologies (FQRNT).

[1]Y. Miyahara, J. Topple, Z. Schumacher, and P. Grutter, Phys. Rev. Appl. **4**, 054011 (2015).
[2]M. Nonnenmacher, M. P. O'Boyle, and H. K. Wickramasinghe, Appl. Phys. Lett. **58**, 2921 (1991).
[3]S. Kitamura, K. Suzuki, M. Iwatsuki, and C. B. Mooney, Appl. Surf. Sci. **157**, 222 (2000).
[4]L. N. Kantorovich, A. I. Livshits, and M. Stoneham, J. Phys.: Condens. Matter **12**, 795 (2000).
[5]A. Labuda, K. Kobayashi, Y. Miyahara, and P. Grütter, Rev. Sci. Instrum. **83**, 053703 (2012).
[6]T. R. Albrecht, P. Grutter, D. Horne, and D. Rugar, J. Appl. Phys. **69**, 668 (1991).
[7]H. Hölscher, B. Gotsmann, W. Allers, U. Schwarz, H. Fuchs, and R. Wiesendanger, Phys. Rev. B **64**, 075402 (2001).
[8]L. N. Kantorovich and T. Trevethan, Phys. Rev. Lett. **93**, 236102 (2004).
[9]J. E. Sader, T. Uchihashi, M. J. Higgins, A. Farrell, Y. Nakayama, and S. P. Jarvis, Nanotechnology **16**, S94 (2005).
[10]Y. Sugawara, L. Kou, Z. Ma, T. Kamijo, Y. Naitoh, and Y. J. Li, Appl. Phys. Lett. **100**, 223104 (2012).
[11]H. Nomura, K. Kawasaki, T. Chikamoto, Y. J. Li, Y. Naitoh, M. Kageshima, and Y. Sugawara, Appl. Phys. Lett. **90**, 033118 (2007).
[12]T. Fukuma, K. Kobayashi, H. Yamada, and K. Matsushige, Rev. Sci. Instrum. **75**, 4589 (2004).
[13]For convenience, HF2LI lock-in amplifier (Zurich Instruments) in external reference mode was used as a frequency doubler as well as phase shifter.
[14]P. Zahl, T. Wagner, R. Möller, and A. Klust, J. Vac. Sci. Technol., B: Nanotechnol. Microelectron. **28**, C4E39 (2010).
[15]T. Hochwitz, A. K. Henning, C. Levey, and C. Daghlian, J. Vac. Sci. Technol., B: Nanotechnol. Microelectron. **14**, 457 (1996).
[16]H. O. Jacobs, P. Leuchtmann, O. J. Homan, and A. Stemmer, J. Appl. Phys. **84**, 1168 (1998).
[17]T. Glatzel, S. Sadewasser, and M. Lux-Steiner, Appl. Surf. Sci. **210**, 84 (2003).
[18]U. Zerweck, C. Loppacher, T. Otto, S. Grafstrom, and L. M. Eng, Phys. Rev. B **71**, 125424 (2005).
[19]H. Diesinger, D. Deresmes, J.-P. Nys, and T. Mélin, Ultramicroscopy **110**, 162 (2010).